One-Step Electrodeposited Nickel Cobalt Sulfide Nanosheet Arrays for High-Performance Asymmetric Supercapacitors

Wei Chen, Chuan Xia, and Husam N. Alshareef*

Materials Science and Engineering, King Abdullah University of Science and Technology (KAUST), Thuwal 23955-6900, Saudi Arabia

ABSTRACT A facile one-step electrodeposition method is developed to prepare ternary nickel cobalt sulfide interconnected nanosheet arrays on conductive carbon substrates as electrodes for supercapacitors, resulting in exceptional energy storage performance. Taking advantages of the highly conductive, mesoporous nature of the nanosheets and open framework of the three-dimensional nanoarchitectures, the ternary sulfide electrodes exhibit high specific capacitance (1418 F g^{-1} at 5 A g^{-1} and 1285 F g^{-1} at 100 A g^{-1}) with excellent rate capability. An asymmetric supercapacitor fabricated by the ternary sulfide nanosheet arrays as positive electrode and porous graphene film as negative electrode demonstrates outstanding electrochemical performance for practical energy storage applications. Our asymmetric supercapacitors show a high energy density of 60 Wh kg^{-1} at a power density of 1.8 kW kg^{-1}. Even when charging the cell within 4.5 s, the energy density is still as high as 33 Wh kg^{-1} at an outstanding power density of 28.8 kW kg^{-1} with robust long-term cycling stability up to 50 000 cycles.

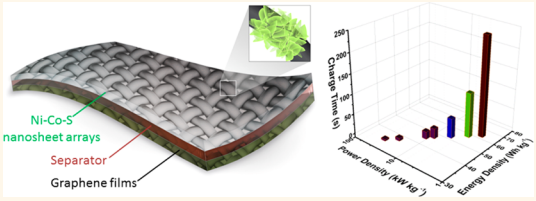

KEYWORDS: nickel cobalt sulfides · interconnected nanosheet arrays · electrochemical deposition · graphene · asymmetric supercapacitors

Development of energy storage devices with high energy and power outputs, long lifetime, and short charging time is urgently needed to meet the increasing demand for energy and power in our daily life.[1−3] Supercapacitors are emerging as very promising energy storage devices with some excellent properties such as high power density, long cycle life, fast charge time, and safe operation mode.[4−6] However, supercapacitors suffer from relatively lower energy density as compared to rechargeable lithium batteries.[4] In recent years, great research progress has been accomplished for the improvement of supercapacitor performance by the fabrication of nanostructured electrode materials.[7,8] Carbon-based materials, transition metal oxides/hydroxides, and conducting polymers are among the most intensively explored supercapacitor materials for energy storage applications.[9−12] Typically, supercapacitors using carbon-based materials (activated carbon, carbon nanotubes, graphene, *etc.*) show low capacitance due to their surface dominant electrochemical double-layer storage mechanism.[13−15] Transition metal oxides, hydroxides (MnO_2, Co_3O_4, MoO_3, $Ni(OH)_2$, *etc.*) and conducting polymers (polyaniline, polypyrrole, poly(3,4-ethylenedioxythiophene), *etc.*) show higher capacitance owing to their redox-reaction-enriched energy storage mechanism. However, these materials have either low conductivity or poor electrochemical stability, a fact that has largely limited their widespread applications in supercapacitors.[16−22] Therefore, it is important to develop new electrode materials with desirable supercapacitor properties, such as high electrical conductivity, porous structure, large capacitance, and good electrochemical stability.

Recently, transition metal sulfides including binary cobalt sulfides, nickel sulfides, copper sulfides, and ternary nickel cobalt sulfides have been investigated as novel supercapacitor electrode materials with improved electrochemical performance.[23−28] Chang *et al.* prepared hollow CoS hexagonal nanosheets by a hydrothermal method, and

* Address correspondence to husam.alshareef@kaust.edu.sa.

Received for review July 11, 2014 and accepted August 18, 2014.

Published online August 18, 2014
10.1021/nn503814y

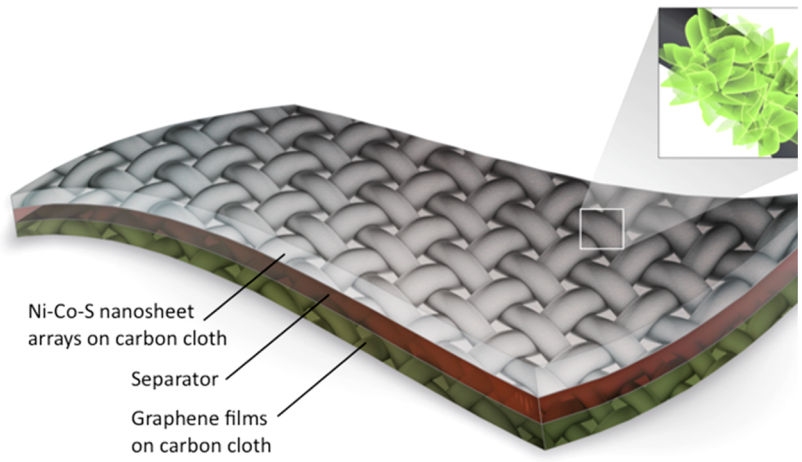

Figure 1. Schematic of the design of asymmetric supercapacitors by applying interconnected Ni−Co−S nanosheet arrays on carbon cloth as a positive electrode and porous graphene film as a negative electrode.

the supercapacitor based on these CoS showed a capacitance of 326.4 F g^{-1} under a high current density of 64.6 A g^{-1} in the three-electrode measurement.[29] Zeng *et al*. synthesized flower-like NiS for supercapacitors with a high specific capacitance of 965.98 F g^{-1} at a current density of 0.5 A g^{-1} in the three-electrode measurement.[30] Lou *et al*. reported a multiple-step and template-engaged method to grow CuS nanoneedles on carbon nanotubes, and the supercapacitor using this composite showed a capacitance of 114 F g^{-1} at a scan rate of 2 mV s^{-1} in the three-electrode test.[31] It was reported that the ternary sulfides such as nickel cobalt sulfides have an electronic conductivity of about 2 orders higher than that of the oxide counterparts and much higher conductivity than those of the binary sulfides.[32−34] In addition, the electrochemical contributions from both nickel and cobalt ions in the ternary sulfides are expected to provide richer redox reactions than that of the single binary sulfides (nickel sulfide or cobalt sulfide), resulting in better electrochemical energy storage performance.[35,36] Recently, Xia *et al*. prepared $NiCo_2S_4$ urchin-like nanostructures by a multistep hydrothermal method that converted the corresponding ternary-based carbonate hydroxide precursors by S^{2-} ion exchange. The supercapacitors based on the $NiCo_2S_4$ urchin-like nanostructures presented a high capacitance of 1149 F g^{-1} at current density of 0.5 A g^{-1} in the three-electrode measurement.[37] Wang *et al*. reported a similar multistep route to grow $NiCo_2S_4$ nanotube arrays on carbon fiber paper by hydrothermal preparation of the carbonate hydroxide precursor, followed by the vulcanization thermal treatment and acid etching processes. The obtained $NiCo_2S_4$ nanotube arrays exhibited a high areal capacitance of 0.87 F cm^{-2} at 4 mA cm^{-2} in the three-electrode measurement.[26] Lou *et al*. developed a two-step sacrificial template method to prepare $Ni_xCo_{3-x}S_4$ hollow nanoprisms that were sulfurized from a Ni−Co precursor. The $NiCo_2S_4$ hollow prisms manifested a high specific capacitance of 895.2 F g^{-1} when tested as supercapacitor material at a current density of 1 A g^{-1} in the three-electrode measurement.[38] Unfortunately, the above-mentioned methods involve multistep processes that make the development of the ternary sulfides costly, complicated, and time-consuming. Moreover, a real-life demonstration of a ternary sulfide based supercapacitor (the practical configuration of two-electrode full cell devices) is essential for energy storage applications, as recently highlighted by Ruoff *et al*.[39]

We herein report the development of ternary nickel cobalt sulfides with controllable composition by a facile one-step electrochemical co-deposition method and their application as positive electrodes for asymmetric supercapacitors with excellent energy storage properties. The hierarchically interconnected ternary sulfide nanosheet arrays grown on conductive carbon cloth exhibit a very high capacitance of 1418 F g^{-1} at a current density of 5 A g^{-1} in the three-electrode measurement, and the capacitance remained as high as 90.6% (1285 F g^{-1}) when the current density increased to 100 A g^{-1}. The asymmetric ternary sulfide//graphene supercapacitor, where the ternary sulfide and graphene act as positive and negative electrodes, respectively, shows a very high energy density of 60 Wh kg^{-1} at a power density of 1.8 kW kg^{-1} with a charge time of 247.7 s. Even under a very short charge time of 4.5 s, the asymmetric supercapacitor still kept a high energy density of 33.3 Wh kg^{-1} at a power density of 28.7 kW kg^{-1}.

RESULTS AND DISCUSSION

The design of the asymmetric supercapacitor with the employment of ternary nickel cobalt sulfide (Ni−Co−S) as the positive electrode and graphene film as the negative electrode is schematically illustrated in Figure 1. It shows that the ternary Ni−Co−S interconnected nanosheet arrays are grown directly on the woven conductive carbon cloth, making the electrode highly porous (macroscopically porous as the whole

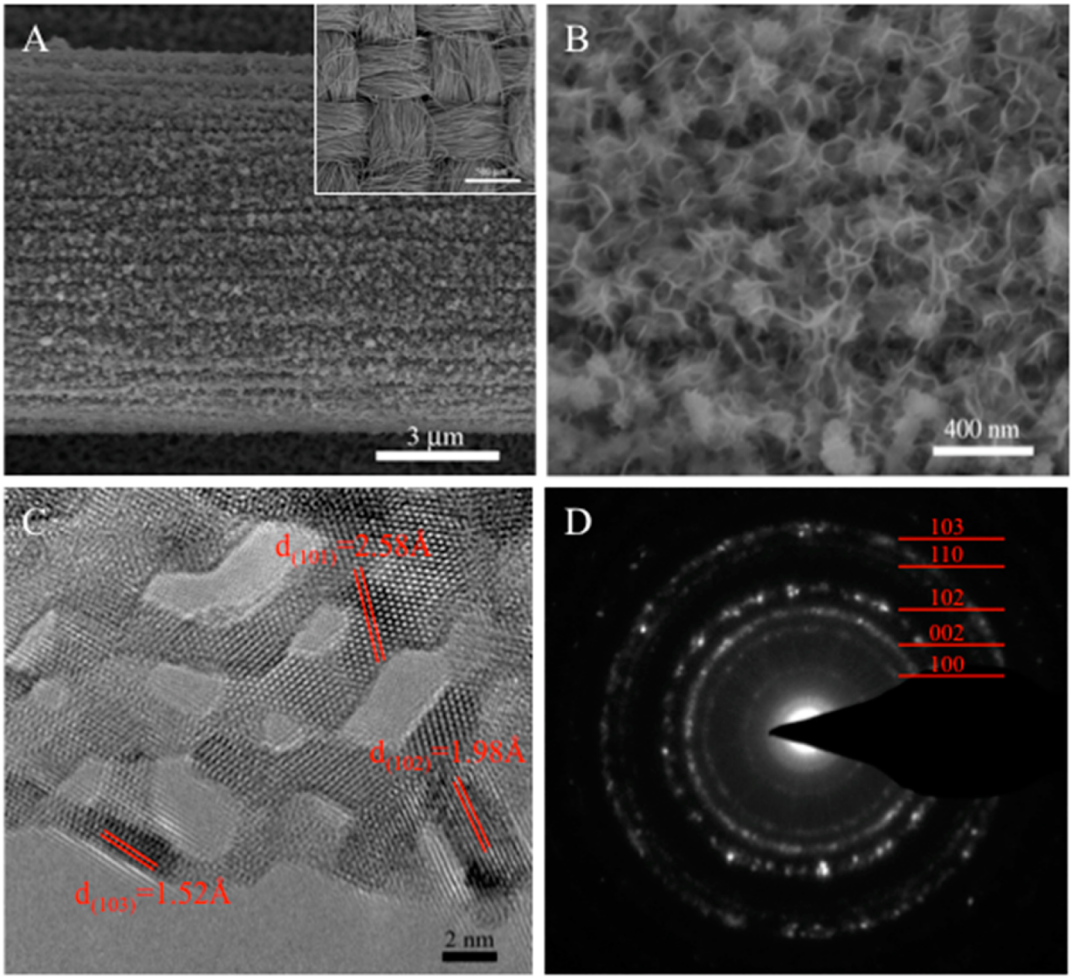

Figure 2. Characterization of the Ni—Co—S-4 nanosheet arrays by SEM (A, B) and TEM (C, D). Scale bar of the inset Figure A is 500 μm.

electrode and nanoscopically porous due to the nanomaterial design). This is believed to facilitate the electrolyte ion trapping and access to the porous structures, which will reduce the electrolyte ion transportation path during the supercapacitor charge—discharge process. In addition, the porous graphene film attached to the carbon cloth acts as an effective negative electrode and further promotes the flow of electrolytes in the whole device.

We are able to control the growth of the as-prepared Ni—Co—S nanosheets by adjusting the concentrations of the electrodeposition solutions. Five different ternary sulfides, henceforth referred to as Ni—Co—S-1 to Ni—Co—S-5, have been investigated which correspond to the different concentrations of the deposition solutions (see Experimental Section for detail). As shown in Figure S1, with the increase of Ni^{2+} concentration at a specific concentration of Co^{2+}, the electrodeposited Ni—Co—S sheets transform from lightly deposited nanosheets with large intersheet gaps (Figure S1A), to moderately deposited nanosheet arrays (Figure S1B), and then to heavily deposited nanosheet arrays (Figure S1C and Figure 2), and finally to excessively deposited nanosheet films with some cracks due to their mechanical expansion (Figure S1D). The deposition of Ni—Co—S nanosheet arrays on the carbon fibers is successfully achieved, as can be differentiated from the smooth surface of the pure carbon cloth fibers (Figure S2). Importantly, the one-step electrodeposition of the ternary sulfides provides a facile and effective approach for large-scale application, which is a distinct advantage compared to other multistep fabrication techniques. The different morphology and composition of the Ni—Co—S nanosheet arrays is expected to give markedly different electrochemical properties when used as a supercapacitor electrode, as will be discussed in the next section. It will be further found that the Ni—Co—S-4 interconnected nanosheet gives the best electrochemical performance as a supercapacitor electrode, and we thus focus on studying this optimized Ni—Co—S electrode in this work.

Figure 2 shows the morphology and microstructure of the optimized Ni—Co—S-4 with different magnifications that are revealed by scanning electron microscopy (SEM) and transmission electron microscopy (TEM). The low-magnification image of the Ni—Co—S on carbon cloth (inset of Figure 2A) shows an overview of the integrated electrode, where the woven conductive

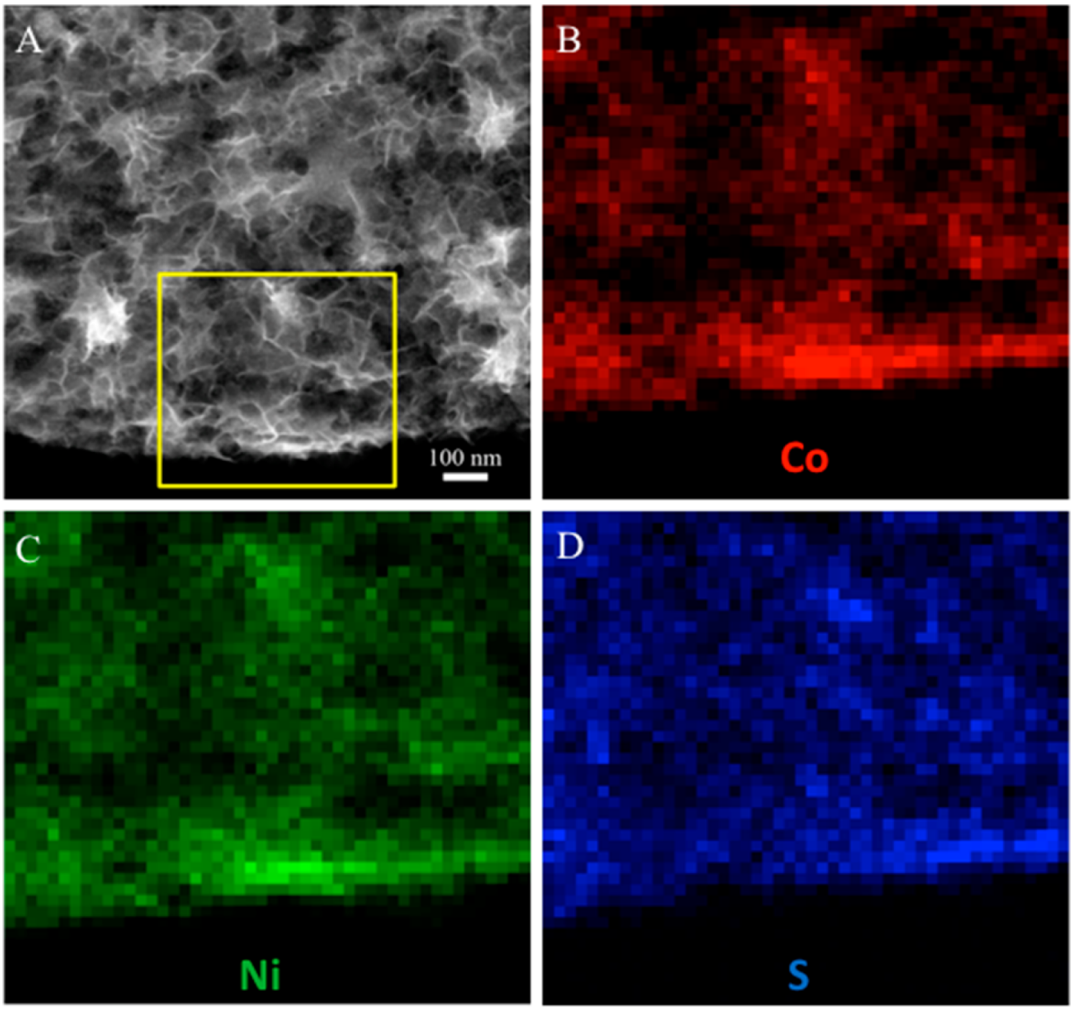

Figure 3. HAADF-STEM image (A) and EDX mapping of the elements (B) cobalt, (C) nickel, and (D) sulfur, respectively.

carbon cloth with a macroporous nature serves as an excellent scaffold for the uniform deposition of the ternary nanosheet arrays (Figure 2A). It is believed that the adhesion of the Ni—Co—S on carbon cloth is very robust due to the uniform material coating and the merits of the electrodeposition technique. Even after heavy deposition of the materials, the resulting electrode retains a good macroporous nature without blocking its macroscopic pores. This morphology is favorable for the effective flow of the electrolyte ions throughout the whole electrode structure, resulting in extensive contact of the electrode materials with the electrolyte ions for enhanced charge storage reactions. A higher magnification SEM image (Figure 2B) demonstrates that the vertically grown Ni—Co—S on a carbon fiber forms a dense array of highly porous nanosheets that are interconnected, as confirmed by a low-magnification TEM image (Figure S3A). Looking into the detail of the Ni—Co—S microstrutures, it is found that in addition to the macroporous nature of the interconnected nanosheet arrays, the ultrathin Ni—Co—S nanosheets themselves are mesoporous in nature (Figure S3B and Figure 2C). As a result, they form a fully porous nanostructured electrode, which is a highly desired morphology for supercapacitor applications. It is further revealed that the size of the mesopores in the Ni—Co—S nanosheet is in the range between 2 and 10 nm (Figure 2C). The highly crystalline lattice fringes with different orientations show that the Ni—Co—S nanosheet is polycrystalline in nature. This is further confirmed by the selected area electron diffraction (SAED) pattern taken on the Ni—Co—S nanosheet (Figure 2D). The indexed lattice fringes in Figure 2C correspond to the Ni—Co—S with a composition of $CoNi_2S_4$, which is consistent with the indexed SAED pattern with different lattice planes. The absence of some lattice planes in Figure 2C that appear in the SAED pattern is probably due to the spatial limitation of the TEM. Similar designs of nanoporous materials with macroporous features have previously been demonstrated as excellent electrodes for supercapacitor energy storage devices.[40—42]

We further employed high-angle annular dark-field scanning transmission electron microscopy (HAADF-STEM) and energy-dispersive X-ray spectroscopy (EDX) mapping to study the elemental distribution in the electrode material of Ni—Co—S nanosheet arrays. The HAADF-STEM image shown in Figure 3A exhibits a

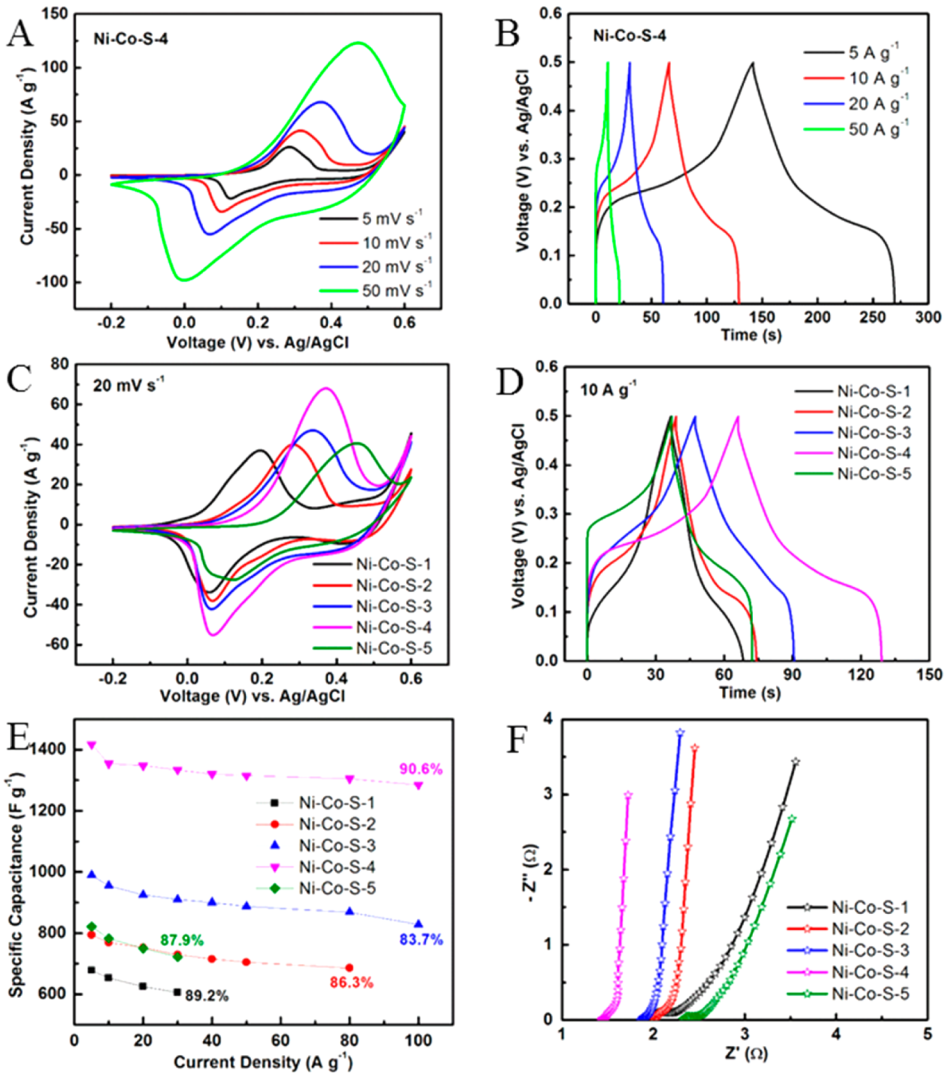

Figure 4. Electrochemical performance of the Ni−Co−S nanosheets as supercapacitor electrodes in the three-electrode measurements with 1 M KOH as the electrolyte. (A) Cyclic voltammetry and (B) galvanostatic charge−discharge curves of the optimized Ni−Co−S-4 nanosheets; (C) cyclic voltammetry, (D) galvanostatic charge−discharge curves, (E) summary of specific capacitance as a function of current density, and (F) Nyquist plot of all the Ni−Co−S electrodes, respectively.

uniform layer of interconnected nanosheets, which agrees well with the SEM observation, as shown in Figure 2B. The EDX-STEM elemental mapping images in Figure 3B−D correspond to the K-edge signals of Co, Ni, and S, respectively. The even distribution of the Co, Ni, and S elements demonstrates the uniform deposition of the Ni−Co−S nanosheet arrays, which further confirms the successful preparation of the ternary Ni−Co−S nanosheets by one-step electrodeposition.

X-ray photoelectron spectroscopy (XPS) analysis was carried out in order to further investigate the chemical composition of the Ni−Co−S nanosheets and the oxidation state of the detected elements. High-resolution XPS spectra of Co 2p, Ni 2p, and S 2p core levels have been recorded and are shown in Figure S4, which match well with those obtained for ternary cobalt nickel sulfides of $CoNi_2S_4$.[43] The Ni $2p_{3/2}$ peaks observed at 853.3 and 856.4 eV are characteristic of Ni^{2+} and Ni^{3+} species (Figure S4A), while the Co $2p_{3/2}$ peaks observed at 778.5 and 781.6 eV are characteristic of Co^{3+} and Co^{2+} species, respectively (Figure S4B).[43,44] For the S 2p high-resolution XPS spectrum (Figure S4C), the peak observed at 161.5 eV corresponding to the S $2p_{3/2}$ core level is typical of metal−sulfur bonds in the ternary metal sulfides and consistent with nickel sulfides and cobalt sulfides.[45−47] The S 2p peak observed at 169.0 eV is attributed to surface sulfur with high oxide state, such as sulfates.[46]

The electrochemical properties of the Ni−Co−S nanosheets as positive electrode were investigated first in the three-electrode measurements with 1 M KOH as the electrolyte. As shown in Figure 4A, the cyclic voltammetry curves obtained under different scan rates show a pair of redox peaks, representing a typical electrochemical behavior of the sulfide electrodes.[38,43] The formation of the redox peaks is probably ascribed to the reactions between the electrode material and the alkaline electrolyte, according to the following

equation:[26,48]

$$CoNi_2S_4 + 2OH^- \leftrightarrow CoS_{2x}OH + Ni_2S_{4-2x}OH + 2e^-$$

The reversible redox reactions give rise to the formation of CoSOH and NiSOH, similar to the reaction mechanism of cobalt sulfides and nickel sulfides as has been previously reported.[24,29] The anodic peaks shift to higher potential while the cathodic peaks shift to lower potential as the scan rate is increased due to the faster charge and discharge rates. The galvanostatic charge–discharge curves show symmetric charge and discharge processes even at high current densities (Figure 4B), indicating the excellent electrochemical features of the ternary sulfides as pseudocapacitor electrodes and their superior rate capability.

The electrochemical performances of Ni–Co–S ternary nanosheets with different compositions were all investigated as pseudocapacitor materials in the alkaline electrolyte. At the same scan rate of 20 mV s^{-1}, the anodic peaks shift to higher potential with the increase of Ni^{2+} concentration in the electrodeposition of Ni–Co–S ternary nanosheets (Figure 4C). This agrees with the electrochemical behaviors of cobalt sulfides and nickel sulfides reported previously, in which the cobalt sulfides showed much lower redox reaction potential compared to that of nickel sulfides due to their intrinsic electrochemical response to the electrolyte.[38,49,50] In addition, the intensity of the current increases with the electrodeposition solution concentration to a maximal value and then decreases, resulting in the optimized electrodeposition condition that we mentioned in the previous section. The high current density induced by the optimized Ni–Co–S-4 nanosheets will give rise to the best energy storage performance among all the studied ternary nanosheets. The charge–discharge curves show symmetric electrochemical characteristics and very small voltage drops in the discharge process, indicating good electrical and ionic conductivity of the ternary sulfides (Figure 4D). As summarized in Figure 4E, the specific capacitances of Ni–Co–S ternary electrodes vary with their different compositions within a large range of current densities. Specifically, the capacitance of the Ni–Co–S ternary electrodes increases with the concentration of Ni^{2+} in the electrodeposition solution at a given concentration of Co^{2+}, while the Ni–Co–S electrode prepared with further increased Ni^{2+} concentration results in much lower capacitance. For example, the specific capacitance of Ni–Co–S-4 nanosheets at 10 A g^{-1} is as high as 1354 F g^{-1}, much higher than that of 653 F g^{-1} for Ni–Co–S-1, 769 F g^{-1} for Ni–Co–S-2, 955 F g^{-1} for Ni–Co–S-3, and 783 F g^{-1} for Ni–Co–S-5. The energy storage performance of the Ni–Co–S electrodes is probably correlated to their unique morphology as well as composition. The very high specific capacitance of 1418 F g^{-1} at 5 A g^{-1} for Ni–Co–S-4 nanosheets is among the highest values reported so far for metal sulfides.[23,27,36–38,48] Impressively, the Ni–Co–S ternary nanosheets prepared by the facile one-step electrodeposition exhibit ultrafast charge and discharge characteristics and outstanding rate capabilities. As for the optimized Ni–Co–S-4 nanosheets, the electrode can even be charged within a few seconds at a very high current density of 100 A g^{-1}, while its specific capacitance can still remain as high as 1285 F g^{-1}. Therefore, it shows a very high rate capability of 90.6%, superior to that of the other Ni–Co–S nanosheets (range from 83.7% to 89.2% as shown in Figure 4E). Moreover, the Ni–Co–S-4 nanosheets show the best conductivity among all the investigated ternary sulfides, as demonstrated by the Nyquist plot in Figure 4F. The excellent electrochemical performance of the Ni–Co–S-4 nanosheets benefits from the following facts. First, the highly conductive Ni–Co–S nanosheets contact directly on the conductive carbon cloths to form an integrated electrode with superb highways for fast electron transportation and electrolyte ion diffusion, which greatly increase the charge rate of the electrode for high-power applications. Second, the interconnected nanosheets with mesoporous nanostructures grown on the macroporous carbon substrate serve as an ideal platform for supercapacitive energy storage. The porous three-dimensional electrode allows facile electrolyte ion access for fast and reversible redox reactions, largely contributing to the increased energy storage capacity for high-energy applications. Third, the unique hierarchical morphology of the Ni–Co–S nanosheet arrays is critical to the long-term stability of energy storage devices. Overall, the successful fabrication of the three-dimensional electrode gains a number of advantages that benefit supercapacitive energy storage devices.

To further explore the electrochemical properties toward practical application of the Ni–Co–S nanosheet arrays, we have fabricated an asymmetric supercapacitor by employing the optimized Ni–Co–S as positive electrode and graphene film as negative electrode. It is well known that graphene is an excellent supercapacitor material, serving as a good negative electrode in alkaline electrolytes due to promising features such as high surface area, good conductivity, and superior electrochemical stability.[51–53] The graphene used in this study was prepared by a facile one-pot hydrothermal method as reported elsewhere.[54,55] As shown in Figure S5, the reduced graphene oxide with a few layers exhibits a wrinkled characteristic that is ideal to serve as a supercapacitor electrode, in which the electrolyte ions have full access to the graphene electrode.[56,57] The electrochemical performance of the graphene electrode was studied in the three-electrode measurement with 1 M KOH as the electrolyte (Figure S6). It is shown that the graphene electrode has excellent electrochemical performance in terms of rectangular cyclic voltammetry curves (Figure S6A),

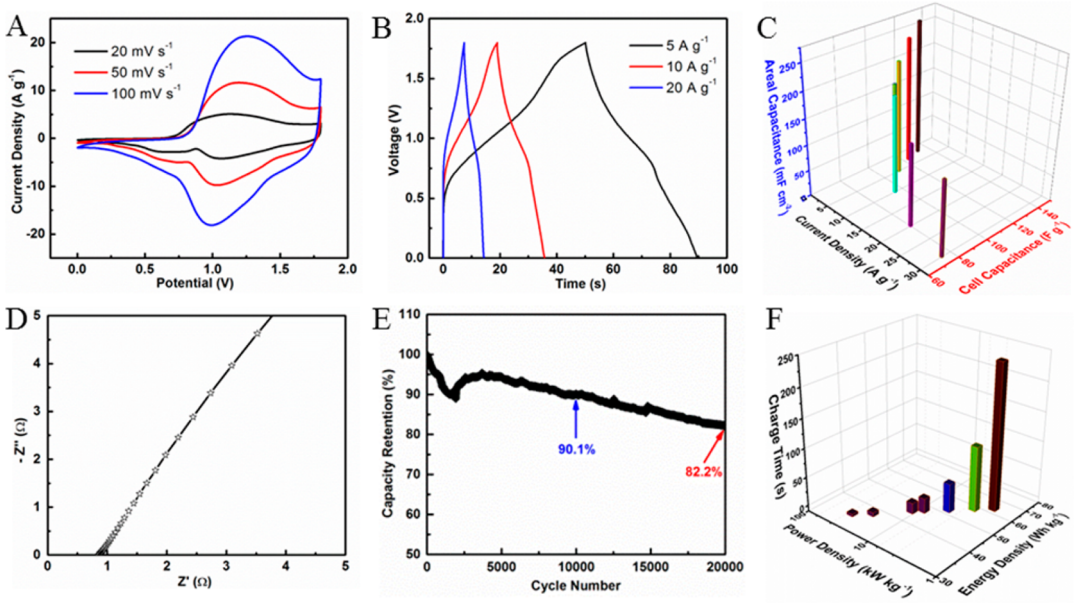

Figure 5. Electrochemical performance of the Ni–Co–S//graphene asymmetric supercapacitors. (A) Cyclic voltammetry curves; (B) galvanostatic charge–discharge curves; (C) cell capacitance and areal capacitance *vs* current density; (D) Nyquist plot; (E) cycling stability performance; (F) Ragone plot (energy density *vs* power density *vs* charge time).

symmetric charge–discharge behaviors (Figure S6B), and long-term cycling stability (Figure S6D). In a prolonged voltage window of 1.2 V (from −1.2 to 0 V), the specific capacitance of the graphene electrode can reach as high as 332 F g^{-1} at a current density of 4 A g^{-1}, and it still remains 171 F g^{-1} at a current density of 100 A g^{-1} (Figure S6C). Moreover, the graphene electrode shows negligible decay of the initial capacitance after 10000 cycles of charge and discharge at a high current density of 40 A g^{-1}. The excellent electrochemical properties of the graphene electrode indicate that it is ideal to act as a negative electrode in this study.

The asymmetric supercapacitor is composed of Ni–Co–S nanosheet arrays as positive electrode, graphene film as negative electrode, and 1 M KOH as electrolyte. The mass loading of the two electrode materials was balanced before making the full cell devices, and the voltage window of the full cell was determined to be 1.8 V, according to their individual electrochemical behaviors (Figure S7; see Experimental Section for details). Figure 5 shows the electrochemical performance of the asymmetric supercapacitors. The cyclic voltammetry curves show a pair of distinct peaks under different scan rates, corresponding to the redox reactions of Ni–Co–S with the alkaline electrolyte (Figure 5A).[48,58] The nearly symmetric charge and discharge curves with very small voltage drops at different current densities are indicative of good supercapacitor behaviors (Figure 5B). As summarized in Figure 5C, the cell capacitance of the asymmetric supercapacitors based on the total masses of the two electrodes is at a very high level, ranging from 74 to 133 F g^{-1}. For example, the cell capacitance is as high as 133 F g^{-1} at a current density of 2 A g^{-1}, while it is still 74 F g^{-1} at a current density of 30 A g^{-1}. The cell capacitances of our asymmetric supercapacitors are the highest reported values so far for sulfide-based asymmetric supercapacitors.[48,58−60] The areal capacitance is an important parameter to indicate the total capacitance of the device that normalized to the geometrical area by a certain amount of electrode material. Our asymmetric supercapacitor shows a relatively high areal capacitance, from 263 mF cm^{-2} at 2 A g^{-1} to 146 mF cm^{-2} at 30 A g^{-1}, demonstrating its good capability to store enough energy in a confined area. The Nyquist plot in Figure 5D represents excellent electrical conductivity of the device with a very small cell resistance (0.86 Ω) shown at a high frequency range. The disappearance of the semicircle in the Nyquist plot in a high frequency range exhibits very small charge-transfer resistance of the device, which is probably ascribed to the integrated 3D electrodes that minimize the contact impedance between electrodes and electrolyte.

As a critical parameter to determine the energy storage performance for practical applications, the long-term cycling stability of our asymmetric sueprcapacitor is tested and shown in Figure 5E. The asymmetric device is capable of retaining 90.1% and 82.2% of the initial capacitance after 10 000 and 20 000 consecutive charge–discharge tests, respectively. The capacitance of the cell degraded slowly with the cycle test; however it still retained 63.2% of the capacitance even after 50 000 cycles (Figure S7). This is the first ultralong cycling test that was applied to the asymmetric supercapacitors, showing the outstanding cycle life of our devices. The cycling stability of our asymmetric supercapacitor is remarkable when compared to previous studies on sulfide-based asymmetric

supercapacitors reported in good studies by Zhang *et al.* (73.1% retention after 3000 cycles for Ni–Co sulfide nanowires//activated carbon cells), Lin *et al.* (90% retention after 5000 cycles for Ni_3S_2-MWCNT// activated carbon cells), and Shen *et al.* (90.2% retention after 2000 cycles for Co_9S_8 nanorod//Co_3O_4@RuO_2 nanosheet based cells). Further, our cycling stability results are highly comparable to those of other asymmetric supercapacitors based on different materials, such as CoO@polypyrrole//activated carbon asymmetric supercapacitors (91.5% retention after 20 000 cycles), $Ni(OH)_2$-CNT//activated carbon asymmetric supercapacitors (83% retention after 3000 cycles), and graphene-MnO_2//SWCNT asymmetric supercapacitors (95% retention after 5000 cycles).[58−63] The capacity decay after long-term cycling for our asymmetric full cells is not well understood yet, but is probably due to the following reasons. First, the positive Ni–Co–S electrode may undergo material evolution and partially change to ternary oxides or hydroxides due to their intensive reactions with the alkaline electrolyte, which decreases their energy storage capacity. Second, the fast and long-term cycling tests may induce the mechanical failure of the Ni–Co–S electrode, resulting in the delamination of the materials from the substrate. Third, the morphology of the interconnected ternary nanosheets may be altered or damaged by the fast and long term cycling tests. Figure 5F shows an advanced Ragone plot of our asymmetric supercapacitors (energy density *vs* power density *vs* charge time). Impressively, our devices show a very high energy density of 60 Wh kg^{-1} at a power density of 1.8 kW kg^{-1}, and the corresponding charge time is only 248 s. Even when charging the cell within 4.5 s, the energy density is still as high as 33 Wh kg^{-1} at an outstanding power density of 28.8 kW kg^{-1}. The obtained high energy and power densities of our supercapacitors are some of the highest values reported so far among asymmetric supercapacitors. For example, Lin *et al.* reported a nice study on Ni_3S_2-MWCNT//activated carbon asymmetric devices, achieving an energy density of 19.8 Wh kg^{-1} at a power density of 798 W kg^{-1}. Zhang *et al.* reported Ni–Co sulfide nanowires//activated carbon cells with an energy density of 25 Wh kg^{-1} at a power density of 447 W kg^{-1}. Gong *et al.* reported $Ni(OH)_2$-CNT//activated carbon asymmetric supercapacitors with an energy density of 50.6 Wh kg^{-1} at a power density of 95 W kg^{-1}. Duan *et al.* showed a MnO_2//graphene asymmetric device with an energy density of 23.2 Wh kg^{-1} at a power density of 1 kW kg^{-1}.[58,60,62,64] The high energy and power density of our asymmetric supercapacitors with very short charge time are of great promise for practical energy storage applications.

CONCLUSIONS

In summary, we have demonstrated a facile, one-step electrodeposition process of nickel cobalt sulfide nanosheet arrays for high-performance asymmetric supercapacitors. The reported electrochemical deposition process of the ternary sulfides is controllable and has a number of advantages over the conventional multistep processes for the preparation of sulfides. The optimized nickel cobalt sulfides with interconnected nanosheet arrays on a conductive carbon substrate serves as an excellent three-dimensional supercapacitor electrode, showing high specific capacitance (1418 F g^{-1} at 5 A g^{-1} and 1285 F g^{-1} at 100 A g^{-1}) and excellent rate capability and conductivity. Furthermore, the asymmetric supercapacitor fabricated by the optimized nickel cobalt sulfide nanosheet arrays as positive electrode and porous graphene film as negative electrode demonstrated outstanding electrochemical performance. Our asymmetric supercapacitors showed high energy and power density with short charge time, as well as robust long-term cycling stability. The performance we achieved suggests that the ternary sulfides prepared by the scalable one-step electrodeposition process have great potential in various energy storage technologies.

EXPERIMENTAL SECTION

Materials. All chemicals used in this study were received from Sigma-Aldrich and used without further treatment. DI water (18.2 MΩ·cm) from Milli Q was used throughout the whole experiment.

Electrochemical Co-deposition of Ni–Co–S Nanosheet Arrays. The Ni–Co–S with different morphology and composition were electrochemically co-deposited onto the flexible carbon cloth with a woven carbon fiber configuration. Prior to the electrodeposition, the carbon cloth was wetted and cleaned with acetone and water, respectively. The electrodeposition solution contains 5 mM $CoCl_2 \cdot 6H_2O$ with different concentrations of $NiCl_2 \cdot 6H_2O$ (1, 2.5, 5, 7.5, and 10 mM) and 0.75 M thiourea ($CS(NH_2)_2$), resulting in the obtained Ni–Co–S electrodes with names of Ni–Co–S-1, Ni–Co–S-2, Ni–Co–S-3, Ni–Co–S-4, and Ni–Co–S-5, respectively. The pH value of the solution was adjusted with diluted $NH_3 \cdot H_2O$ to ~6. The electrodynamic deposition was carried out in a three-electrode cell using cleaned carbon cloth as the working electrode, Pt as counter electrode, and Ag/AgCl as reference electrode by cyclic voltammetry at a scan rate of 5 mV s^{-1} for 15 cycles within a voltage range of −1.2 to 0.2 V *vs* Ag/AgCl. The electrodeposited carbon cloth was cleaned by rinsing with a large amount of water, followed by drying in air for 12 h and vacuum drying at 80 °C for 12 h. The mass loading of the Ni–Co–S on the carbon cloth was determined by the mass difference before and after the electrodeposition using a microbalance (Mettler Toledo XP26, resolution of 1 μg). The typical mass loading of the positive Ni–Co–S-4 electrode is about 0.8 mg/cm^2.

Preparation of Graphene Films. The graphene films were prepared according to a modified method reported by the Dan Li group.[57,65] Specifically, the graphene oxide (GO) prepared by a modified Hummer's method was dispersed in water with a concentration of 0.5 mg mL^{-1}. The GO solution was subject

to bath sonication for 2 h (Branson 2510), followed by ultrasonication at 160 W (UP400S, ultrasonic processor, Hielscher) for another 1 h. The GO solution was then centrifuged at 3000 rpm for 30 min to remove any unexfoliated GO. The pH value of the obtained GO dispersion was adjusted to ~10 by $NH_3 \cdot H_2O$. We used a hydrothermal reaction to reduce the GO and produce a well-dispersed graphene solution, namely, hydrothermally reduced graphene oxide (HTrGO), which was reported by our and other studies elsewhere.[54−56] Subsequently, the HTrGO dispersion was vacuum filtered through an AAO membrane (pore size of 0.2 μm). The vacuum filter was disconnected immediately after no dispersion was left. The filtered graphene film on the AAO membrane was transferred to water, and the graphene film can be easily peeled off from the membrane. The graphene film was then attached to the carbon cloth and used as a negative electrode for the asymmetric supercapacitor.

Fabrication of Ni−Co−S//Graphene Asymmetric Supercapacitors. The fabrication of the Ni−Co−S//graphene asymmetric supercapacitors was conducted by taking the Ni−Co−S nanosheet arrays and graphene films as positive and negative electrodes, respectively. A 1 M KOH solution was used as the electrolyte, and a porous polymer membrane as the separator (Celgard 3501). The asymmetric supercapacitors were assembled in pouch cells by sealing them into plastic bags to avoid evaporation of the aqueous electrolyte during the long-time measurement. Prior to the fabrication of the asymmetric supercapacitor, the masses of the positive and negative electrodes were balanced according to the following equation:[66]

$$\frac{m_+}{m_-} = \frac{C_{s-}\Delta V_-}{C_{s+}\Delta V_+}$$

where m is the mass, C_s is the specific capacitance, and ΔV is the voltage range for positive (+) and negative (−) electrodes, respectively. The typical mass loading of an asymmetric supercapacitor is about 2.6 mg/cm^2.

Material Characterization. The morphology and microstructure of the samples were characterized by SEM (Nova Nano 630, FEI) and TEM (Titan 80−300 kV (ST) TEM, FEI). The XPS analysis was conducted on a Kratos AXIS Ultra DLD spectrometer.

Electrochemical Measurements. The electrochemical tests were carried out at room temperature in both three-electrode (half-cell) and two-electrode (full-cell) configurations. In the three-electrode measurements, Ni−Co−S deposited on the carbon cloth was used as the working electrode, a Pt wire as the counter electrode, and Ag/AgCl as the reference electrode. In the full-cell measurement, an asymmetric supercapacitor with Ni−Co−S acting as positive electrode and graphene film as negative electrode was assembled in the pouch cells. A 1 M KOH solution was used as electrolyte for all electrochemical measurements. The electrochemical performance was tested in a VMP3 multichannel electrochemical workstation (Bio-Logic) by the techniques of electrochemical impedance spectroscopy (EIS), cyclic voltammetry (CV), and galvanostatic charge−discharge (CD). The voltage window is from −0.2 to 0.6 V *vs* Ag/AgCl for the positive Ni−Co−S electrode, −1.2 to 0 V *vs* Ag/AgCl for the negative graphene electrode, and thus 0 to 1.8 V for the asymmetric Ni−Co−S//graphene cell.

The capacitance values were calculated from galvanostatic charge−discharge curves according to the following equations:

half-cell:

$$C_s = \frac{I}{\frac{\Delta V}{\Delta t}m}$$

full cell:

$$C_{cell} = \frac{I}{\frac{\Delta V}{\Delta t}M}$$

where the specific capacitance (C_s) applies to a single electrode and the cell capacitance (C_{cell}) applies to the full cell only, I is the applied current in the measurement, ($\Delta V/\Delta t$) is the slope of discharge curve after the voltage drop, m is the mass of the active materials on the single electrodes, and M is the total mass of the active materials on both the positive and negative electrodes ($M = m_+ + m_-$).

The calculation of energy and power density is based on the total weight of the two electrodes in the full-cell devices according to the following equations.

$$E = \frac{1}{2}C_{cell}V^2$$

$$P = \frac{E}{t_d} = \frac{1}{2}C_{cell}V^2/t_d$$

where E is energy density, P is the power density, C_{cell} is the cell capacitance, V is the maximum voltage applied during the charge−discharge measurement, and t_d is the discharge time obtained from the discharge curve.

Conflict of Interest: The authors declare no competing financial interest.

Acknowledgment. Research reported in this publication has been supported by King Abdullah University of Science and Technology (KAUST). The authors wish to thank the staff of the Imaging and Characterization Laboratory at KAUST, especially Dr. Qingxiao Wang for his help with the TEM analysis and Dr. Nejib Hedhili for his help with the XPS measurements. The authors also thank Dr. Rakhi RaghavanBaby from the Functional Nanomaterials and Devices Group at KAUST for several useful discussions.

Supporting Information Available: Additional SEM, TEM, XPS, and electrochemical performance results. This material is available free of charge *via* the Internet at http://pubs.acs.org.

REFERENCES AND NOTES

1. Armand, M.; Tarascon, J. M. Building Better Batteries. *Nature* **2008**, *451*, 652–657.
2. Tarascon, J. M.; Armand, M. Issues and Challenges Facing Rechargeable Lithium Batteries. *Nature* **2001**, *414*, 359–367.
3. Arico, A. S.; Bruce, P.; Scrosati, B.; Tarascon, J. M.; Van Schalkwijk, W. Nanostructured Materials for Advanced Energy Conversion and Storage Devices. *Nat. Mater.* **2005**, *4*, 366–377.
4. Simon, P.; Gogotsi, Y. Materials for Electrochemical Capacitors. *Nat. Mater.* **2008**, *7*, 845–854.
5. Kotz, R.; Carlen, M. Principles and Applications of Electrochemical Capacitors. *Electrochim. Acta* **2000**, *45*, 2483–2498.
6. Winter, M.; Brodd, R. J. What Are Batteries, Fuel Cells, and Supercapacitors? *Chem. Rev.* **2004**, *104*, 4245–4269.
7. Liu, C.; Li, F.; Ma, L.-P.; Cheng, H.-M. Advanced Materials for Energy Storage. *Adv. Mater.* **2010**, *22*, E28–E62.
8. Wang, G.; Zhang, L.; Zhang, J. A Review of Electrode Materials for Electrochemical Supercapacitors. *Chem. Soc. Rev.* **2012**, *41*, 797–828.
9. Frackowiak, E. Carbon Materials for Supercapacitor Application. *Phys. Chem. Chem. Phys.* **2007**, *9*, 1774–1785.
10. Futaba, D. N.; Hata, K.; Yamada, T.; Hiraoka, T.; Hayamizu, Y.; Kakudate, Y.; Tanaike, O.; Hatori, H.; Yumura, M.; Iijima, S. Shape-Engineerable and Highly Densely Packed Single-Walled Carbon Nanotubes and Their Application as Super-Capacitor Electrodes. *Nat. Mater.* **2006**, *5*, 987–994.
11. Pandolfo, A. G.; Hollenkamp, A. F. Carbon Properties and Their Role in Supercapacitors. *J. Power Sources* **2006**, *157*, 11–27.
12. Lang, X.; Hirata, A.; Fujita, T.; Chen, M. Nanoporous Metal/Oxide Hybrid Electrodes for Electrochemical Supercapacitors. *Nat. Nanotechnol.* **2011**, *6*, 232–236.
13. Chmiola, J.; Yushin, G.; Gogotsi, Y.; Portet, C.; Simon, P.; Taberna, P. L. Anomalous Increase in Carbon Capacitance at Pore Sizes Less Than 1 Nanometer. *Science* **2006**, *313*, 1760–1763.
14. Lee, J.; Kim, J.; Hyeon, T. Recent Progress in the Synthesis of Porous Carbon Materials. *Adv. Mater.* **2006**, *18*, 2073–2094.

15. Frackowiak, E.; Beguin, F. Electrochemical Storage of Energy in Carbon Nanotubes and Nanostructured Carbons. *Carbon* **2002**, *40*, 1775–1787.
16. Hall, P. J.; Mirzaeian, M.; Fletcher, S. I.; Sillars, F. B.; Rennie, A. J. R.; Shitta-Bey, G. O.; Wilson, G.; Cruden, A.; Carter, R. Energy Storage in Electrochemical Capacitors: Designing Functional Materials to Improve Performance. *Energy Environ. Sci.* **2010**, *3*, 1238–1251.
17. Jiang, J.; Li, Y.; Liu, J.; Huang, X.; Yuan, C.; Lou, X. W. Recent Advances in Metal Oxide-Based Electrode Architecture Design for Electrochemical Energy Storage. *Adv. Mater.* **2012**, *24*, 5166–5180.
18. Wei, W.; Cui, X.; Chen, W.; Ivey, D. G. Manganese Oxide-Based Materials as Electrochemical Supercapacitor Electrodes. *Chem. Soc. Rev.* **2011**, *40*, 1697–1721.
19. Snook, G. A.; Kao, P.; Best, A. S. Conducting-Polymer-Based Supercapacitor Devices and Electrodes. *J. Power Sources* **2011**, *196*, 1–12.
20. Rakhi, R. B.; Chen, W.; Cha, D.; Alshareef, H. N. Substrate Dependent Self-Organization of Mesoporous Cobalt Oxide Nanowires with Remarkable Pseudocapacitance. *Nano Lett.* **2012**, *12*, 2559–2567.
21. Toupin, M.; Brousse, T.; Belanger, D. Charge Storage Mechanism of MnO_2 Electrode Used in Aqueous Electrochemical Capacitor. *Chem. Mater.* **2004**, *16*, 3184–3190.
22. Chen, W.; Rakhi, R. B.; Wang, Q.; Hedhili, M. N.; Alshareef, H. N. Morphological and Electrochemical Cycling Effects in MnO_2 Nanostructures by 3D Electron Tomography. *Adv. Funct. Mater.* **2014**, *24*, 3130–3143.
23. Tao, F.; Zhao, Y. Q.; Zhang, G. Q.; Li, H. L. Electrochemical Characterization on Cobalt Sulfide for Electrochemical Supercapacitors. *Electrochem. Commun.* **2007**, *9*, 1282–1287.
24. Chou, S. W.; Lin, J. Y. Cathodic Deposition of Flaky Nickel Sulfide Nanostructure as an Electroactive Material for High-Performance Supercapacitors. *J. Electrochem. Soc.* **2013**, *160*, D178–D182.
25. Raj, C. J.; Kim, B. C.; Cho, W. J.; Lee, W. G.; Seo, Y.; Yu, K. H. Electrochemical Capacitor Behavior of Copper Sulfide (CuS) Nanoplatelets. *J. Alloys Compd.* **2014**, *586*, 191–196.
26. Xiao, J.; Wan, L.; Yang, S.; Xiao, F.; Wang, S. Design Hierarchical Electrodes with Highly Conductive $NiCo_2S_4$ Nanotube Arrays Grown on Carbon Fiber Paper for High-Performance Pseudocapacitors. *Nano Lett.* **2014**, *14*, 831–838.
27. Lin, J.-Y.; Chou, S.-W. Cathodic Deposition of Interlaced Nanosheet-Like Cobalt Sulfide Films for High-Performance Supercapacitors. *RSC Adv.* **2013**, *3*, 2043–2048.
28. Wang, Q.; Jiao, L.; Du, H.; Yang, J.; Huan, Q.; Peng, W.; Si, Y.; Wang, Y.; Yuan, H. Facile Synthesis and Superior Supercapacitor Performances of Three-Dimensional Cobalt Sulfide Hierarchitectures. *CrystEngComm* **2011**, *13*, 6960–6963.
29. Yang, Z.; Chen, C.-Y.; Chang, H.-T. Supercapacitors Incorporating Hollow Cobalt Sulfide Hexagonal Nanosheets. *J. Power Sources* **2011**, *196*, 7874–7877.
30. Yang, J.; Duan, X.; Qin, Q.; Zheng, W. Solvothermal Synthesis of Hierarchical Flower-Like Beta-NiS with Excellent Electrochemical Performance for Supercapacitors. *J. Mater. Chem. A* **2013**, *1*, 7880–7884.
31. Zhu, T.; Xia, B.; Zhou, L.; Wen Lou, X. Arrays of Ultrafine CuS Nanoneedles Supported on a CNT Backbone for Application in Supercapacitors. *J. Mater. Chem.* **2012**, *22*, 7851–7855.
32. Zhang, G.; Lou, X. W. Controlled Growth of $NiCo_2O_4$ Nanorods and Ultrathin Nanosheets on Carbon Nanofibers for High-Performance Supercapacitors. *Sci. Rep.* **2013**, *3*, 1–6.
33. Huang, L.; Chen, D.; Ding, Y.; Feng, S.; Wang, Z. L.; Liu, M. Nickel−Cobalt Hydroxide Nanosheets Coated on $NiCo_2O_4$ Nanowires Grown on Carbon Fiber Paper for High-Performance Pseudocapacitors. *Nano Lett.* **2013**, *13*, 3135–3139.
34. Xiao, J.; Zeng, X.; Chen, W.; Xiao, F.; Wang, S. High Electrocatalytic Activity of Self-Standing Hollow $NiCo_2S_4$ Single Crystalline Nanorod Arrays towards Sulfide Redox Shuttles in Quantum Dot-Sensitized Solar Cells. *Chem. Commun.* **2013**, *49*, 11734–11736.
35. Liu, Q.; Jin, J.; Zhang, J. $NiCo_2S_4$@Graphene as a Bifunctional Electrocatalyst for Oxygen Reduction and Evolution Reactions. *ACS Appl. Mater. Interfaces* **2013**, *5*, 5002–5008.
36. Peng, S.; Li, L.; Li, C.; Tan, H.; Cai, R.; Yu, H.; Mhaisalkar, S.; Srinivasan, M.; Ramakrishna, S.; Yan, Q. *In Situ* Growth of $NiCo_2S_4$ Nanosheets on Graphene for High-Performance Supercapacitors. *Chem. Commun.* **2013**, *49*, 10178–10180.
37. Chen, H.; Jiang, J.; Zhang, L.; Wan, H.; Qi, T.; Xia, D. Highly Conductive $NiCo_2S_4$ Urchin-Like Nanostructures for High-Rate Pseudocapacitors. *Nanoscale* **2013**, *5*, 8879–8883.
38. Yu, L.; Zhang, L.; Wu, H. B.; Lou, X. W. Formation of $Ni_xCo_{3-x}S_4$ Hollow Nanoprisms with Enhanced Pseudocapacitive Properties. *Angew. Chem., Int. Ed.* **2014**, *53*, 3711–3714.
39. Stoller, M. D.; Ruoff, R. S. Best Practice Methods for Determining an Electrode Material's Performance for Ultracapacitors. *Energy Environ. Sci.* **2010**, *3*, 1294–1301.
40. Guan, C.; Li, X.; Wang, Z.; Cao, X.; Soci, C.; Zhang, H.; Fan, H. J. Nanoporous Walls on Macroporous Foam: Rational Design of Electrodes to Push Areal Pseudocapacitance. *Adv. Mater.* **2012**, *24*, 4186–4190.
41. Yang, L.; Cheng, S.; Ding, Y.; Zhu, X.; Wang, Z. L.; Liu, M. Hierarchical Network Architectures of Carbon Fiber Paper Supported Cobalt Oxide Nanonet for High-Capacity Pseudocapacitors. *Nano Lett.* **2011**, *12*, 321–325.
42. Chen, W.; Rakhi, R. B.; Hu, L.; Xie, X.; Cui, Y.; Alshareef, H. N. High-Performance Nanostructured Supercapacitors on a Sponge. *Nano Lett.* **2011**, *11*, 5165–5172.
43. Du, W.; Wang, Z.; Zhu, Z.; Hu, S.; Zhu, X.; Shi, Y.; Pang, H.; Qian, X. Facile Synthesis and Superior Electrochemical Performances of $CoNi_2S_4$/Graphene Nanocomposite Suitable for Supercapacitor Electrodes. *J. Mater. Chem. A* **2014**, *2*, 9613–9619.
44. Prabu, M.; Ketpang, K.; Shanmugam, S. Hierarchical Nanostructured $NiCo_2O_4$ as an Efficient Bifunctional Non-Precious Metal Catalyst for Rechargeable Zinc-Air Batteries. *Nanoscale* **2014**, *6*, 3173–3181.
45. Ohno, Y. Electronic Structure of the Misfit-Layer Compounds PbTiS and SnNbS. *Phys. Rev. B* **1991**, *44*, 1281–1291.
46. Legrand, D. L.; Nesbitt, H. W.; Bancroft, G. M. X-Ray Photoelectron Spectroscopic Study of a Pristine Millerite (NiS) Surface and the Effect of Air and Water Oxidation. *Am. Mineral.* **1998**, *83*, 1256–1265.
47. Lin, J.-Y.; Liao, J.-H. Mesoporous Electrodeposited-CoS Film as a Counter Electrode Catalyst in Dye-Sensitized Solar. *J. Electrochem. Soc.* **2012**, *159*, D65–D71.
48. Chen, H. C.; Jiang, J. J.; Zhang, L.; Xia, D. D.; Zhao, Y. D.; Guo, D. Q.; Qi, T.; Wan, H. Z. *In Situ* Growth of $CoNi_2S_4$ Nanotube Arrays on Ni Foam for Supercapacitors: Maximizing Utilization Efficiency at High Mass Loading to Achieve Ultrahigh Areal Pseudocapacitance. *J. Power Sources* **2014**, *254*, 249–257.
49. Zhou, W.; Cao, X.; Zeng, Z.; Shi, W.; Zhu, Y.; Yan, Q.; Liu, H.; Wang, J.; Zhang, H. One-Step Synthesis of Ni_3S_2 Nanorod@$Ni(OH)_2$ Nanosheet Core-Shell Nanostructures on a Three-Dimensional Graphene Network for High-Performance Supercapacitors. *Energy Environ. Sci.* **2013**, *6*, 2216–2221.
50. Xia, X.; Zhu, C.; Luo, J.; Zeng, Z.; Guan, C.; Ng, C. F.; Zhang, H.; Fan, H. J. Synthesis of Free-Standing Metal Sulfide Nanoarrays *via* Anion Exchange Reaction and Their Electrochemical Energy Storage Application. *Small* **2014**, *10*, 766–773.
51. Wang, Y.; Shi, Z.; Huang, Y.; Ma, Y.; Wang, C.; Chen, M.; Chen, Y. Supercapacitor Devices Based on Graphene Materials. *J. Phys. Chem. C* **2009**, *113*, 13103–13107.
52. Zhu, Y.; Murali, S.; Stoller, M. D.; Ganesh, K. J.; Cai, W.; Ferreira, P. J.; Pirkle, A.; Wallace, R. M.; Cychosz, K. A.; Thommes, M.; *et al.* Carbon-Based Supercapacitors Produced by Activation of Graphene. *Science* **2011**, *332*, 1537–1541.
53. Huang, Y.; Liang, J.; Chen, Y. An Overview of the Applications of Graphene-Based Materials in Supercapacitors. *Small* **2012**, *8*, 1805–1834.
54. Bai, Y.; Rakhi, R. B.; Chen, W.; Alshareef, H. N. Effect of Ph-Induced Chemical Modification of Hydrothermally

Reduced Graphene Oxide on Supercapacitor Performance. *J. Power Sources* **2013**, *233*, 313–319.
55. Xu, Y.; Sheng, K.; Li, C.; Shi, G. Self-Assembled Graphene Hydrogel *via* a One-Step Hydrothermal Process. *ACS Nano* **2010**, *4*, 4324–4330.
56. Chen, W.; Rakhi, R. B.; Alshareef, H. N. Capacitance Enhancement of Polyaniline Coated Curved-Graphene Supercapacitors in a Redox-Active Electrolyte. *Nanoscale* **2013**, *5*, 4134–4138.
57. Yang, X.; Zhu, J.; Qiu, L.; Li, D. Bioinspired Effective Prevention of Restacking in Multilayered Graphene Films: Towards the Next Generation of High-Performance Supercapacitors. *Adv. Mater.* **2011**, *23*, 2833–2838.
58. Li, Y. H.; Cao, L. J.; Qiao, L.; Zhou, M.; Yang, Y.; Xiao, P.; Zhang, Y. H. Ni-Co Sulfide Nanowires on Nickel Foam with Ultrahigh Capacitance for Asymmetric Supercapacitors. *J. Mater. Chem. A* **2014**, *2*, 6540–6548.
59. Xu, J.; Wang, Q.; Wang, X.; Xiang, Q.; Liang, B.; Chen, D.; Shen, G. Flexible Asymmetric Supercapacitors Based Upon Co_9S_8 Nanorod//Co_3O_4@RuO_2 Nanosheet Arrays on Carbon Cloth. *ACS Nano* **2013**, *7*, 5453–5462.
60. Dai, C.-S.; Chien, P.-Y.; Lin, J.-Y.; Chou, S.-W.; Wu, W.-K.; Li, P.-H.; Wu, K.-Y.; Lin, T.-W. Hierarchically Structured Ni_3S_2/Carbon Nanotube Composites as High Performance Cathode Materials for Asymmetric Supercapacitors. *ACS Appl. Mater. Interfaces* **2013**, *5*, 12168–12174.
61. Zhou, C.; Zhang, Y.; Li, Y.; Liu, J. Construction of High-Capacitance 3D CoO@Polypyrrole Nanowire Array Electrode for Aqueous Asymmetric Supercapacitor. *Nano Lett.* **2013**, *13*, 2078–2085.
62. Tang, Z.; Tang, C.-h.; Gong, H. A High Energy Density Asymmetric Supercapacitor from Nano-Architectured $Ni(OH)_2$/Carbon Nanotube Electrodes. *Adv. Funct. Mater.* **2012**, *22*, 1272–1278.
63. Yu, G.; Hu, L.; Vosgueritchian, M.; Wang, H.; Xie, X.; McDonough, J. R.; Cui, X.; Cui, Y.; Bao, Z. Solution-Processed Graphene/MnO_2 Nanostructured Textiles for High-Performance Electrochemical Capacitors. *Nano Lett.* **2011**, *11*, 2905–2911.
64. Gao, H.; Xiao, F.; Ching, C. B.; Duan, H. High-Performance Asymmetric Supercapacitor Based on Graphene Hydrogel and Nanostructured MnO_2. *ACS Appl. Mater. Interfaces* **2012**, *4*, 2801–2810.
65. Li, D.; Muller, M. B.; Gilje, S.; Kaner, R. B.; Wallace, G. G. Processable Aqueous Dispersions of Graphene Nanosheets. *Nat. Nanotechnol.* **2008**, *3*, 101–105.
66. Yan, J.; Fan, Z.; Sun, W.; Ning, G.; Wei, T.; Zhang, Q.; Zhang, R.; Zhi, L.; Wei, F. Advanced Asymmetric Supercapacitors Based on $Ni(OH)_2$/Graphene and Porous Graphene Electrodes with High Energy Density. *Adv. Funct. Mater.* **2012**, *22*, 2632–2641.